J. Schmitz[a], J. Brillo[a], I. Egry[a], R. Schmid-Fetzer[b]
[a] Institut für Materialphysik im Weltraum, Deutsches Zentrum für Luft- und Raumfahrt, Köln, Germany
[b] Institut für Metallurgie, Technische Universität Clausthal, Clausthal-Zellerfeld, Germany

# Surface tension of liquid Al–Cu binary alloys



Surface tension data of liquid Al–Cu binary alloys have been measured contactlessly using the technique of electromagnetic levitation. A digital CMOS-camera (400 fps) recorded image sequences of the oscillating liquid sample and surface tensions were determined from analysis of the frequency spectra.

Measurements were performed for samples covering the entire range of composition and precise data were obtained in a broad temperature range.

It was found that the surface tensions can be described as linear functions of temperature with a negative slope. Moreover, they monotonically decrease with an increase in the aluminium concentration. The observed behaviour with respect to both temperature and concentration is in agreement with thermodynamic model calculations using the subregular solution approximation.

**Keywords:** Al–Cu liquid binary alloys; Butler equation; Multilayer model; Segregation; Surface tension

## 1. Introduction

### 1.1. Al–Cu

Liquid Al–Cu alloys play an important role in lightweight casting and, due to the presence of low temperature eutectic compositions, in lead-free soldering [1, 2].

Both of these processes are dominated by bulk, surface- and interface phenomena. The corresponding thermophysical properties therefore need to be known precisely. Moreover, with increasing availability of computer power, the quality of the simulations of technical casting and welding processes is limited mainly by the accuracy of thermophysical input parameters [3, 4].

Reliable systematic information exists, for this system, on density and thermal expansion [5–8] measured recently by us. It already becomes clear from these data that Al–Cu is a strongly interacting system with a highly non-ideal mixing behaviour. Therefore, it is expected to exhibit a non-ideal behavior with respect to surface tension, too.

In the past, surface tension data have been measured by Eremenko [9], Laty [10], as well as Speiser and Poirer [11] using the maximum bubble pressure and the sessile drop method and they reported evidence for associate formation in the melt affecting the surface tension.

It is a particular advantage of the technique of electromagnetic levitation [12] that liquid samples can be processed contactlessly. This avoids contamination of the material due to contact with container walls. In combination with the oscillating drop technique [13], electromagnetic levitation is particularly suited for the measurement of surface tension of liquid Al–Cu – a material highly sensitive to oxygen impurities.

For these reasons it is the goal of the present work not only to update and reassess the existing (older) set of surface tension data for Al–Cu, but also to complete the information for Al-based alloys that we have gathered so far [5–8, 14–17].

### 1.2. Butler and multilayer model

Data measured in this work will be compared to the Butler [18–21] and the multilayer model [22].

In the Butler model, the surface of the liquid is considered as a monolayer of atoms. It is regarded as an individual thermodynamic phase which is in equilibrium with the bulk phase.

As an outcome, numerical information on the surface tension of the alloy and the concentration, $x_i^S$, of a component, $i$, in the surface layer is obtained for a temperature $T$ and bulk concentration $x_i^B$.

The multilayer model describes the surface-near region as a stack of several atomic layers. The atoms are assumed to reside on the sites of a cubic lattice with coordination number 12. The composition of each layer $n$ is calculated using a Monte-Carlo algorithm upon minimization of the surface excess free energy as described in detail in Ref. [22]. The multilayer model provides information on the surface tension and the surface compositions, i.e. the concentration $x_i^{(n)}$ of component $i$ in layer $n$.

Both models require as input parameters the surface tensions, $\gamma_i$, of the pure components, their density, and the excess Gibbs energy, ${}^{E}G^{B}$, of the bulk phase. For a binary alloy A-B, ${}^{E}G^{B}$ is usually written in Redlich–Kister form with temperature dependent parameters ${}^{\nu}L_{A,B}(T)$ [23–25]

$$ {}^{E}G^{B}(x_A^B, T) = x_A^B(1 - x_A^B)\sum_{\nu=0} {}^{\nu}L_{A,B}(T)(2x_A^B - 1)^{\nu} \qquad (1) $$

where $x_i^B$ ($i$ = A, B) denotes the concentration of component $i$ in the bulk phase with $x_A^B + x_B^B = 1$.

The main assumption of the Butler model is the approximation of the surface excess Gibbs energy by [19]

$$ {}^{E}G^{S}(T, x_i^S) \approx \xi \cdot {}^{E}G^{B}(T, x_i^S) \qquad (2) $$

with a phenomenological factor $\xi$ taken as $\xi = 0.66$ in this work, according to Ref. [20]. In a crude way, this approximation accounts for the reduced coordination number of atoms in the surface layer. Surface ordering effects are excluded.

On the other hand, the coordination number of the surface layer is fixed to 9 in the multilayer model due to the underlying cubic lattice. For the same reason, only pair-wise

interactions are taken into account which is equivalent to considering only ${}^0L_{A,B}$ and ${}^1L_{A,B}$ in the Redlich-Kister expansion. A comparison of the two models is discussed in detail in Ref. [16].

## 2. Experimental

### 2.1. Electromagnetic levitation

For the measurement of surface tension data the purity of the surface is of enormous importance [26, 27]. The technique of electromagnetic levitation [12] allows contactless investigations and avoids contamination of the sample material from contact with container walls.

Experiments are performed in a standard stainless steel high vacuum chamber which is filled after evacuation with 600 mbar He with 8 vol.% $H_2$ acting as a reducing agent. A typical sample has an almost spherical shape with a diameter of approximately 5 mm. It is positioned in the centre of the levitation coil to which an alternating current of typically 200 A is applied with a frequency of 300 kHz. The levitation coil consists of two opposed semi-coils 15 mm apart from each other. They generate an inhomogeneous magnetic field which induces eddy currents inside the electrically conductive sample. With a suitable choice of the coil shape, the sample can be positioned stably against gravity. Due to ohmic losses, the induced eddy currents also heat and melt the sample. As levitation and heating are not decoupled, a certain desired temperature can only be adjusted by cooling in a laminar flow of the He/8 %-$H_2$ gas provided by an alumina nozzle underneath the sample.

### 2.2. Temperature measurement

The temperature of the sample is measured by a pyrometer focussed at the sample from the top. As the emissivity is generally not known, the pyrometer output signal, $T_P$, has to be recalibrated with respect to the liquidus temperature $T_L$ of the sample. This is done under the assumption that within the operating wavelength range of the pyrometer the emissivity of the specimen material remains constant with temperature. This is a good approximation for most liquid metals [28]. The droplet temperature $T$ is determined from the following expression derived from Wien's law:

$$\frac{1}{T} - \frac{1}{T_P} = \frac{1}{T_L} - \frac{1}{T_{L,P}} \tag{3}$$

Here, $T_{L,P}$ denotes the pyrometer signal at liquidus temperature. It is identified by a kink in $T_P$ at that time when the melting process is completed and the temperature starts to rise with a steeper slope.

### 2.3. Oscillating drop method

The surface tension, $\gamma$, is determined by means of the oscillating drop method [13]. This technique is based on the fact that surface tension acts as a restoring force for surface oscillations of a liquid droplet. Their frequencies thus serve as a direct measure of the surface tension. This was first studied by Rayleigh [29] for spherical non-rotating droplets. He showed that the square of the so called Rayleigh frequency, $\omega_R$, is proportional to the surface tension. These findings have also been validated for liquid metals under microgravity conditions [30].

Under electromagnetic levitation the sample shape is elongated slightly in the vertical direction and is not spherical anymore. Thus, $\omega_R$ splits up into a set of five frequencies $\omega_m$ with $m = -2, -1, 0, 1, 2$.

They are measured by recording images of the oscillating drop with a high resolution C-MOS camera with 400 frames per second.

The subsequent analysis with an edge detection algorithm produces frequency spectra such as the two shown in Fig. 1. They are Fourier transforms of the difference and the sum signal of two perpendicular radii. Using a symmetry rule, the peaks at $\omega_m$, marked by arrows in Fig. 1, can be identified [13]. The surface tension, $\gamma$, is calculated from these frequencies using the formula of Cummings and Blackburn [31]:

$$\gamma = \frac{3M}{160\pi} \sum_{m=-2}^{2} \omega_m^2 - 1.9\Omega^2 - 0.3\left(\frac{g}{a}\right)^2 \Omega^{-2} \tag{4}$$

Here $M$ is the mass of the sample and $a$ its radius as calculated from $M$ and density for an assumed spherical shape, $g$ is the gravitational constant. In Eq. (4), the parameter $\Omega$ corrects for the magnetic pressure. It is calculated from the three translational frequencies, $\omega_{X,Y,Z}$, that correspond to the horizontal and vertical movements of the sample: $\Omega^2 = 1/3(\omega_x^2 + \omega_y^2 + \omega_z^2)$.

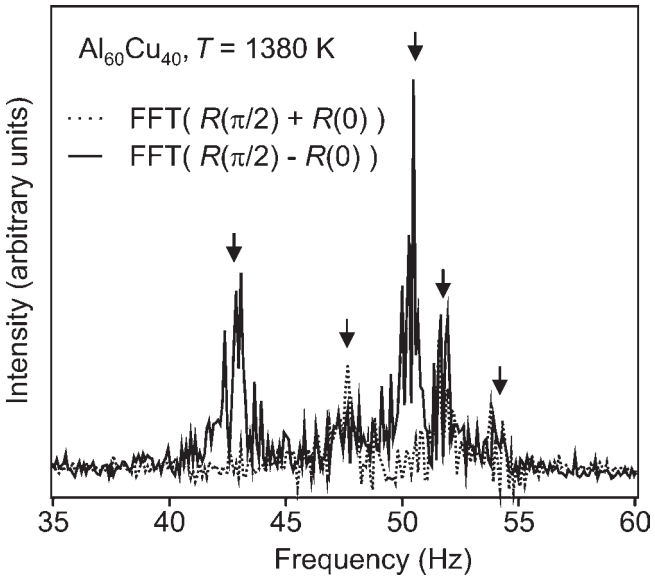


Fig. 1. Typical frequency spectra of the surface oscillations of a liquid $Al_{60}Cu_{40}$ sample at $T = 1380$ K. Solid curve: Fourier transformation of the difference signal of two perpendicular radii. Dotted curve: Fourier transformation of the sum signal of two perpendicular radii.

### 2.4. Sample preparation

Samples were made from pieces of Al and Cu with a purity of 99.999 %. The desired mass was adjusted by pinching the Al and by grinding the Cu pieces. Grinding of Al was avoided as we noticed that this caused contamination of the material. When the correct mass was obtained they were stuck together mechanically using a pair of pliers. Alloying was performed prior to the actual experiment in the levita-

tion furnace by heating to 1700 K. The processing at elevated temperatures also led to an additional cleaning of the material and bright visible oxide spots were removed effectively by their evaporation. The sample mass was determined before the alloying step and right after the measurement. It was found that even when high temperatures were applied, the mean relative mass loss was less than 1.0 %.

### 2.5. Liquidus and experimental temperature range

In order to apply Eq. (3) the liquidus temperature needs to be known precisely. In principle, $T_L$ could be taken from published phase diagram collections but we want to assure that the underlying thermodynamic basis is consistent with the model applications for the surface tension. Therefore, the liquidus temperature is calculated using the description in the COST-507 report [25]. The same data for the liquid phase were also used to calculate the excess Gibbs energy, ${}^{E}G^{B}$, in Eq. (1) for the Butler equation and the multilayer model. These parameters are compiled in Table 1.

Figure 2 shows the resulting liquidus temperature. The various solid phases are not specified in the diagram, but may also be obtained from the complete phase diagram calculation. The temperature ranges covered by the present study are superimposed in Fig. 2 for each investigated alloy composition and compiled in Table 2 for each of the samples. It should be noted that the applied minimum temperature for Cu, $Al_{10}Cu_{90}$, and $Al_{30}Cu_{70}$ is partially lower than the corresponding liquidus temperature $T_L$. This is due to the fact that it was possible to undercool these samples a few Kelvins.

We are aware of the more recent thermodynamic Al–Cu description by Witusiewicz et al. [24]. Above 600 K the data and correspondingly calculated phase diagrams including the liquidus are virtually identical to the earlier COST-507 data. Below 500 K an artefact is observed, not shown in the published COST-507 phase diagram range: the $\gamma$-$D8_3$ stability range widens unrealistically down to room temperature. This

Table 1. Redlich–Kister parameters for liquid Al–Cu [25].

| Parameter | Value (J mol$^{-1}$) |
|---|---|
| ${}^{0}L_{Al,Cu}$ | $-66\,622 + 8.1 \cdot T$ |
| ${}^{1}L_{Al,Cu}$ | $46\,800 - 90.8 \cdot T + 10\,T\ln(T)$ |
| ${}^{2}L_{Al,Cu}$ | $-2812$ |

Table 2. Parameters $T_L$, $\gamma_L$, $\gamma_T$, and $\gamma$(1373 K) for each sample with corresponding uncertainties. The values in bold are the effective temperature range and the corresponding averages respectively. The data for liquid Al were taken from Ref. [6].

| System | $T_L$ (K) | $T_{min}$ (K) | $T_{max}$ (K) | $\gamma_L$ (N m$^{-1}$) | $\gamma_T$ ($10^{-4}$ N (m K)$^{-1}$) | $\gamma$ at 1373 K (N m$^{-1}$) |
|---|---|---|---|---|---|---|
| Cu | 1358 | **1331** | **1686** | **1.30 ± 0.01** | **−2.64 ± 0.9** | **1.31 ± 0.03** |
| $Al_{10}Cu_{90}$ | 1347 | 1360 | 1706 | 1.35 ± 0.004 | −1.96 ± 0.2 | 1.34 ± 0.004 |
| | | 1319 | 1669 | 1.34 ± 0.005 | −2.38 ± 0.3 | 1.33 ± 0.01 |
| | | **1319** | **1706** | **1.35 ± 0.005** | **−2.10 ± 0.2** | **1.34 ± 0.01** |
| $Al_{17}Cu_{83}$ | 1317 | 1339 | 1751 | 1.33 ± 0.007 | −3.83 ± 0.3 | 1.31 ± 0.01 |
| | | 1325 | 1734 | 1.30 ± 0.006 | −1.81 ± 0.3 | 1.29 ± 0.01 |
| | | 1338 | 1706 | 1.33 ± 0.014 | −3.01 ± 0.6 | 1.31 ± 0.02 |
| | | **1325** | **1751** | **1.32 ± 0.013** | **−2.74 ± 0.4** | **1.30 ± 0.01** |
| $Al_{30}Cu_{70}$ | 1304 | 1316 | 1700 | 1.18 ± 0.016 | −0.94 ± 0.7 | 1.17 ± 0.03 |
| | | 1295 | 1719 | 1.21 ± 0.013 | −2.88 ± 0.6 | 1.19 ± 0.03 |
| | | 1305 | 1715 | 1.18 ± 0.010 | −0.59 ± 0.4 | 1.18 ± 0.02 |
| | | **1295** | **1719** | **1.19 ± 0.01** | **−1.30 ± 0.6** | **1.17 ± 0.03** |
| $Al_{40}Cu_{60}$ | 1228 | 1238 | 1638 | 1.12 ± 0.006 | −1.09 ± 0.2 | 1.10 ± 0.01 |
| | | 1249 | 1653 | 1.14 ± 0.004 | −1.77 ± 0.2 | 1.11 ± 0.01 |
| | | 1237 | 1630 | 1.12 ± 0.007 | −1.26 ± 0.3 | 1.10 ± 0.02 |
| | | **1237** | **1653** | **1.13 ± 0.01** | **−1.54 ± 0.2** | **1.11 ± 0.01** |
| $Al_{50}Cu_{50}$ | 1106 | 1112 | 1644 | 1.04 ± 0.011 | −0.73 ± 0.3 | 1.02 ± 0.02 |
| | | 1117 | 1707 | 1.03 ± 0.003 | −0.74 ± 0.1 | 1.01 ± 0.01 |
| | | **1112** | **1707** | **1.04 ± 0.01** | **−0.74 ± 0.2** | **1.01 ± 0.01** |
| $Al_{60}Cu_{40}$ | 980 | 1131 | 1842 | 1.00 ± 0.011 | −0.72 ± 0.2 | 0.97 ± 0.02 |
| | | 1165 | 1748 | 1.00 ± 0.011 | −0.56 ± 0.2 | 0.98 ± 0.02 |
| | | 1202 | 1890 | 1.01 ± 0.007 | −0.59 ± 0.1 | 0.99 ± 0.01 |
| | | 1380 | 1870 | 0.98 ± 0.013 | −0.53 ± 0.2 | 0.95 ± 0.01 |
| | | **1131** | **1890** | **1.00 ± 0.010** | **−0.60 ± 0.2** | **0.97 ± 0.02** |
| $Al_{70}Cu_{30}$ | 867 | 1113 | 1611 | 0.951 ± 0.015 | −0.92 ± 0.3 | 0.90 ± 0.02 |
| | | 1110 | 1519 | 0.974 ± 0.015 | −1.34 ± 0.3 | 0.91 ± 0.02 |
| | | 1123 | 1571 | 0.972 ± 0.010 | −1.11 ± 0.2 | 0.92 ± 0.01 |
| | | **1110** | **1611** | **0.967 ± 0.01** | **−1.11 ± 0.3** | **0.91 ± 0.02** |
| $Al_{83}Cu_{17}$ | 825 | 1053 | 1643 | 0.925 ± 0.018 | −1.73 ± 0.3 | 0.83 ± 0.03 |
| | | 1124 | 1671 | 0.936 ± 0.027 | −1.30 ± 0.5 | 0.87 ± 0.03 |
| | | 1081 | 1612 | 0.953 ± 0.015 | −1.63 ± 0.3 | 0.86 ± 0.02 |
| | | **1053** | **1671** | **0.941 ± 0.02** | **−1.61 ± 0.4** | **0.86 ± 0.03** |
| $Al_{90}Cu_{10}$ | 873 | 1097 | 1609 | 0.912 ± 0.018 | −1.75 ± 0.3 | 0.83 ± 0.03 |
| | | 1093 | 1594 | 0.859 ± 0.010 | −0.99 ± 0.2 | 0.81 ± 0.01 |
| | | 1088 | 1571 | 0.870 ± 0.014 | −1.28 ± 0.3 | 0.81 ± 0.02 |
| | | **1088** | **1609** | **0.871 ± 0.01** | **−1.20 ± 0.3** | **0.81 ± 0.02** |
| Al | 933 | | | 0.87 | −1.55 | 0.80 |

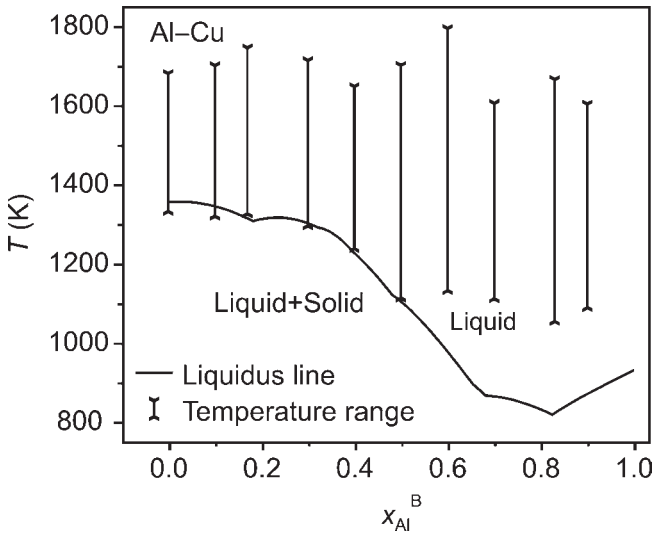


Fig. 2. Calculated liquidus temperatures of Al–Cu; vertical lines denote the temperature range covered by experiments in this study.

artefact is successfully removed in the recent amendment to the dataset [24]. For the liquid phase, however, more adjustable parameters were used in the amendment [24] by introducing an additional Redlich–Kister term, ${}^{3}L_{Al,Cu}$. The calculated liquid enthalpy data are only marginally closer to the experimental data in the temperature range of interest. Since in the current temperature–composition region the differences are not perceivable, the simpler thermodynamic description [25] has been used.

## 3. Results

Measurements of surface tension data were performed for liquid Al–Cu samples in a broad temperature range of $1100\ \mathrm{K} \le T \le 1900\ \mathrm{K}$ and with the bulk aluminium mole fraction, $x_{Al}^{B}$, ranging in small steps from 0 to 1. For each composition up to four different samples were investigated. As mentioned above, a slight undercooling was achieved for Cu, $Al_{10}Cu_{90}$, and $Al_{30}Cu_{70}$.

The obtained surface tensions, $\gamma(T)$, are plotted in Fig. 3 versus temperature. Data of samples with nominally the same composition can be reproduced within approximately 1.6 %. Obviously, the surface tensions can be described as linear functions of temperature with negative slopes and, hence, the following equation can be fitted:

$$\gamma(T) = \gamma_L + \gamma_T(T - T_L) \qquad (5)$$

The parameters $\gamma_L$ and $\gamma_T$ denote in Eq. (5) surface tension at $T_L$ and the temperature coefficient respectively. They are listed for each sample in Table 2 together with their corresponding uncertainties and mean values. In Fig. 3, the scatter for pure copper seems large due to a few single freak values. Nevertheless, Table 2 shows for pure Cu that the deviation in $\gamma_L$ is $\pm 0.01\ \mathrm{N\ m^{-1}}$, which is approximately the same as for all other samples, i.e. it is not significantly increased.

For the pure elements the parameters $\gamma_L$ and $\gamma_T$ are compared in Table 3 with corresponding results from literature [6, 10, 32–40]. The overall agreement with the literature data is good. For liquid Cu the maximum deviation of two values from each other is less than 3 % for $\gamma_L$ and approximately 25 % for $\gamma_T$ if the exceptional value of Ref. [10] is ignored. These deviations are even smaller for liquid Al where $\gamma_L$ scatters within 0.5 % around $0.87\ \mathrm{N\ m^{-1}}$. As discussed in Ref. [41], this value corresponds to a case where only chemisorbed oxygen is present at the surface that is desorbed for $T = 1373$ K.

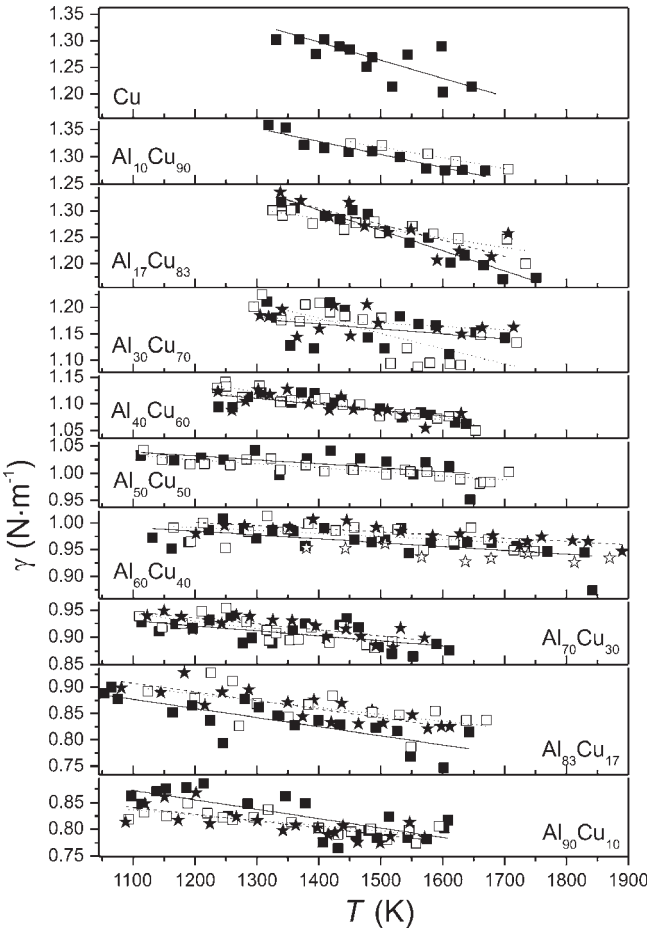


Fig. 3. Measured surface tensions, $\gamma$, of liquid Al–Cu samples versus temperature $T$. Different symbols denote series of experiments with different samples, lines represent the linear regression of each dataset.

Table 3. Parameters $\gamma_L$, and $\gamma_T$, of copper and aluminium in comparison with data reported in various studies.

| Material | $\gamma_L$ (N m$^{-1}$) | $\gamma_T$ ($10^{-4}$ N (m K)$^{-1}$) | Reference |
|---|---|---|---|
| Al | 0.865 | −1.2 | [32] |
| | 0.873 | −1.2 | [33] |
| | 0.865 | −1.5 | [10] |
| | 0.865 | −2.0 | [34] |
| | 0.873 | −1.5 | [35] |
| | 0.865 | −1.6 | [36] |
| | 0.870 | −1.5 | [37] |
| | 0.865 | −1.4 | [9] |
| | 0.871 | −1.55 | [6] |
| Cu | 1.33 | −2.3 | [6] |
| | 1.304 | −2.86 | [38] |
| | 1.29 | −2.3 | [39] |
| | 1.30 | −2.5 | [40] |
| | 1.29 | −1.6 | [10] |
| | 1.30 | −2.64 | this work |

With the use of $\gamma_L$ and $\gamma_T$, the surface tensions are calculated for each sample for $T = 1373$ K. This temperature was chosen for two reasons: First, it lies almost in the centre of the temperature range investigated and second, the results can be directly compared with the literature data [9–11] reported for this temperature as well.

Figure 4 shows the result, $\gamma(T = 1373\ \mathrm{K})$, as a function of the bulk aluminium mole fraction, $x^B_{Al}$. The error bars are of similar size to the symbols and almost hidden by them. Starting in the diagram on the Cu–rich side, the surface tension, $\gamma$, appears to increase slightly from the value of pure copper, 1.3 N m$^{-1}$, to approximately 1.35 N m$^{-1}$ as $x^B_{Al}$ increases to 0.2. After this initial rise, $\gamma$ monotonically decreases with further increasing $x^B_{Al}$. It finally reaches a value of $\gamma = 0.8$ N m$^{-1}$ which corresponds to the surface tension of pure liquid aluminium at this temperature. The data show reasonable agreement with the data of Laty et al. [10] shown in the same figure as well. Their data exhibit the same qualitative behaviour with the following few differences: On the aluminium–rich side, $0.6 \le x^B_{Al} \le 0.97$, they appear slightly smaller than our results and on the copper–rich side, $0.1 \le x^B_{Al} \le 0.2$, they are even significantly smaller so that there is a shoulder in between. The data of Laty et al. [10] also agree with measurements performed by Eremenko [9] who observed the shoulder as well.

The temperature coefficient of the surface tension, $\gamma_T$, for which we found generally negative values, is plotted in Fig. 5 versus $x^B_{Al}$. $\gamma_T$ increases with $x^B_{Al}$ from initially $-2.6 \cdot 10^{-4}$ N m$^{-1}$ K$^{-1}$ to approximately $-1.5 \cdot 10^{-4}$ N m$^{-1}$ K$^{-1}$ for $x^B_{Al} \le 0.4$. $\gamma_T$ remains practically constant on this level for values of $x^B_{Al}$ larger than 0.4 although one might also identify a weak maximum at $x^B_{Al} \approx 0.6$.

In addition, Fig. 5 shows the sessile drop and maximum bubble pressure data measured by Laty et al. [10]. The agreement is particularly good on the aluminium–rich side, i.e. for $x^B_{Al} > 0.5$. Laty reported positive values of $\gamma_T$ for $0.3 \le x^B_{Al} \le 0.4$ and, on the copper–rich side, they report values around $-1.5 \cdot 10^{-4}$ N m$^{-1}$ K$^{-1}$ slightly larger than ours.

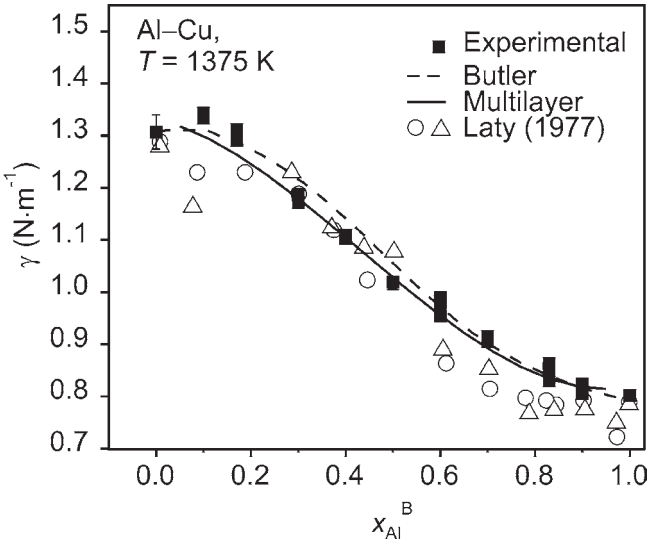


Fig. 4. Surface tension data versus aluminium bulk mole fraction, $x^B_{Al}$ interpolated for each dataset from Eq. (5) for 1375 K (solid squares). The value for pure Al was taken from Ref. [6]. Shown for comparison are values from Ref. [10] measured by means of the sessile drop (triangles) and maximum bubble pressure techniques (circles) as well as calculations for the Butler equation (dashed line) and the multilayer model (solid line).

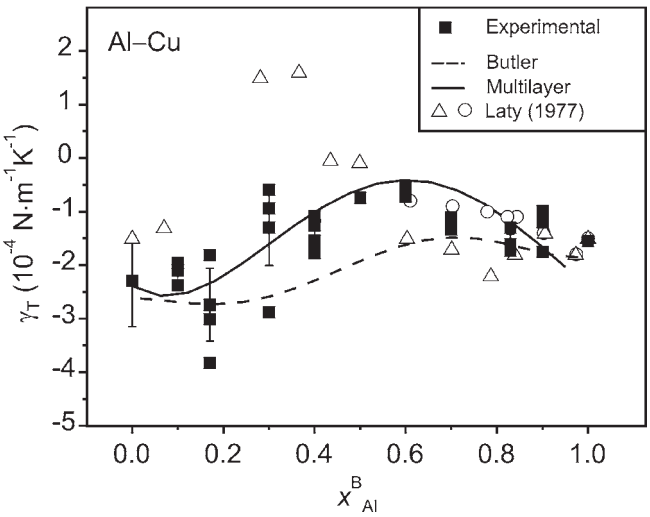


Fig. 5. Thermal coefficient $\gamma_T$ versus $x^B_{Al}$ (solid squares) for each dataset. The value for pure Al was taken from Ref. [6]. Shown for comparison are values from Ref. [10] measured by means of the sessile drop (triangles) and maximum bubble pressure techniques (circles) as well as calculations for the Butler equation (dashed line) and the multilayer model (solid line).

## 4. Discussion

For Al–Cu alloys the obtained data are shown in Fig. 4 together with calculations of the Butler and the multilayer model. For the entire composition range, they both reproduce equally well the experimental data of this work. They also describe the literature values for $0.2 \le x^B_{Al} \le 0.5$ shown in the figure as well.

By performing the calculations for different temperatures, the temperature coefficient of the surface tension, $\gamma_T$, is also predicted as shown in Fig. 5 together with the experimental results. The agreement between the data and the calculation is reasonably good. However, a slightly better agreement with $\gamma_T$, even with respect to the scatter of the data, is obtained from the multilayer model, see Fig. 5. It also seems to reproduce the indicated weak maximum around $x^B_{Al} \approx 0.6$.

In contrast to Laty et al. [10], we did not find any evidence for positive values of $\gamma_T$ and no evidence for positive $\gamma_T$ was reported by Eremenko either [9]. The reason for this discrepancy is probably that the electromagnetic levitation technique provides an environment in which contamination of the sample due to direct contact with solid surfaces is avoided. On the other hand it is well known that traces of impurities such as oxygen can lead to a typical temperature behaviour of $\gamma$ with $\gamma_T > 0$ below a certain temperature [32].

Figure 6 shows segregation profiles, $x^{(n)}_{Al}$ versus $x^B_{Al}$, calculated from the Butler equation, and the multilayer model. Generally, segregation of aluminium in the topmost monolayer, $x^{(1)}_{Al} \ge x^B_{Al}$, is found. With increasing $x^B_{Al}$, $x^{(1)}_{Al}$ increases strongly and becomes larger than 0.8 even for moderate bulk concentrations of $x^B_{Al} \ge 0.5$. The Butler and the multilayer model predict both the same segregation behaviour in $x^{(1)}_{Al}$, where for $x^B_{Al} < 0.6$ the mole fraction of aluminium in the surface mono-

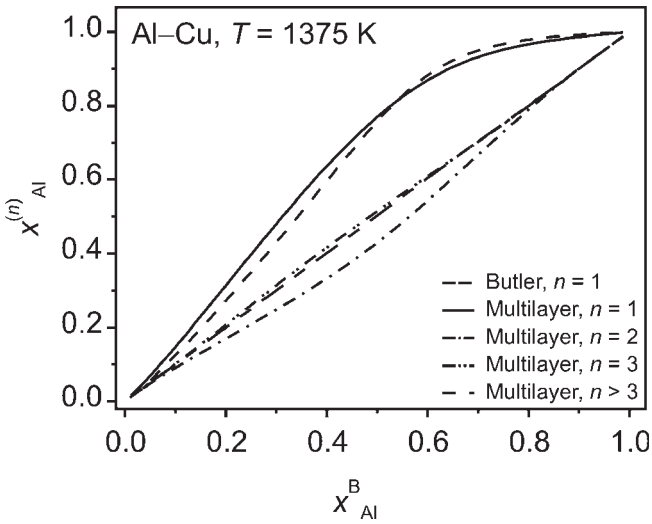


Fig. 6. Calculated segregation profile for 1375 K. The diagram shows the concentration of aluminium in the top monolayer as a function of the bulk concentration calculated for the Butler equation and the multilayer model. The concentrations in the second, third, and fourth layers are also shown.

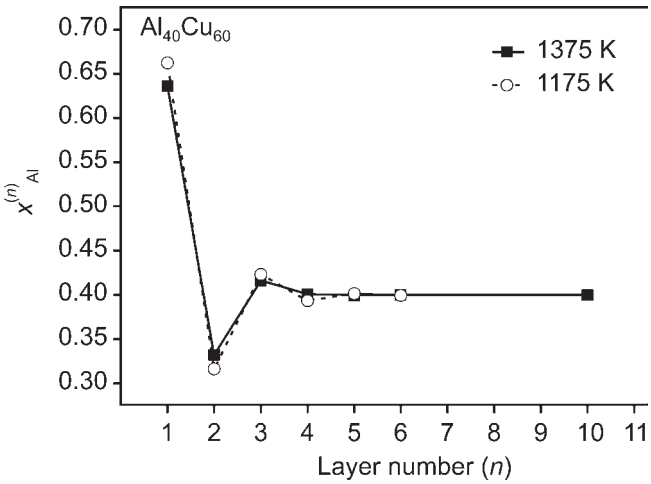


Fig. 7. Calculated concentration profile of aluminium in surface near layers of $Al_{40}Cu_{60}$ alloy for 1375 K and 1175 K.

layer, $x_{Al}^{(1)}$, increases almost linearly with $x_{Al}^{B}$ with a slope larger than 1.

It is a particular advantage of the multilayer model that information can be obtained on the composition of layers below the surface. This is demonstrated in Fig. 6 for the first four layers. In contrast to the top layer, the aluminium concentration is decreased in the second layer with respect to the bulk composition: $x_{Al}^{(2)} \leq x_{Al}^{B}$. The concentration of aluminium in third layer is slightly increased again. The bulk concentration is nearly reached in layers with $n > 3$. This behaviour is further explored in Fig. 7 for $Al_{40}Cu_{60}$ at 1375 K and 1175 K. The plot shows $x_{Al}^{(n)}$ as a function of the layer number $n$. As can be seen, the aluminium concentration oscillates around its bulk value in the surface near region. The effect is slightly increased at 1175 K. These oscillations are caused by the attractive interaction between unlike atoms: as aluminium segregates to the surface, a surplus of copper in the second layer will energetically be favoured due to the negative excess enthalpy. Such a chemical layering, already known from solid surfaces [42, 43], is just one feature of a surface or interface induced order in the liquid. The overall result of these findings is an additional contribution to the surface entropy. This is probably also the reason why the prediction of the Butler equation is not as accurate for $\gamma_T$ as of the multilayer model which at least takes chemical layering into account.

The shoulder in the surface tension data of Eremenko and Laty, Fig. 4, has been interpreted as a sign of associate formation, namely $AlCu_3$, in the melt [9, 10]. On the basis of the experimental data of the present work such a shoulder is not evident. In addition, the Butler equation and the multilayer model describe the experimental findings correctly without including associate formation. In addition, reviewing the thermodynamics of liquid Al–Cu alloys shows no evidence for associate formation near 75 at.% Cu. A necessary condition of short range order, no matter whether it is described by the associate model, quasi-chemical model etc, is a kink or at least strong curvature at the corresponding composition in the enthalpy of mixing curve. The compiled experimental data [24] show nothing like that.

Hence, it can be concluded that associate formation, if it takes place in liquid Al–Cu alloys at all, can be ignored for the description of the surface tension data of this particular system.

## 5. Conclusions

Precise surface tension data have been measured for liquid Al–Cu alloys for the entire range of composition. Measurements were performed in a broad temperature range and linear temperature dependence was observed for all compositions. Moreover, $\gamma$ decreases monotonically with $x_{Al}^{B}$.

There is a reasonably good agreement with results of earlier data; however, reported indications of associate formation could not be confirmed. Instead, we found good agreement with the Butler and the multilayer models, both based on the subregular solution approximation. In addition, the multilayer model was also capable of correctly describing the thermal coefficient of the surface tension.

Both models predict the same moderate segregation behaviour of aluminium at the surface. In addition, the multilayer model indicates that a chemical layering takes place with an oscillatory segregation profile vertical to the surface.

The support by the "Deutsche Forschungsgemeinschaft" (grants BR 3665/1-1 and SCHM 588/31-1) is gratefully acknowledged.

**References**

[1] S.A. David, J.M. Vitek: Int. Mater. Rev. 34 (1989) 213.
[2] S.L. Lehoczky: J. Appl. Phys. 49 (1978) 5479. DOI:10.1063/1.324518
[3] A. Farzadi, M. Do-Quang, S. Serajzadeh, A.H. Kokabi, G. Amberg: Modelling Simul. Mater. Sci. Eng. 16 (2008) 065005. DOI:10.1088/0965-0393/16/6/065005
[4] I. Egry, R. Brooks, D. Holland-Moritz, R. Novakovic, T. Matsushita, E. Ricci, S. Seetharaman, R. Wunderlich, D. Jarvis: Int. J. Thermophys. 28 (2007) 1026. DOI:10.1007/s10765-007-0219-6
[5] T. Iida, R.I.L. Guthrie: Handbook of Physico-chemical Properties at High Temperatures, ISIJ, Edited by The 140th Commitee of Japan Society for Promotion of Science. Tokoyo, Japan, 88.
[6] K.C. Mills: Recommended values of thermophysical properties for selected commercial alloys, Woodhead Publishing Ltd., Cambridge, UK, 2002.
[7] D.M. Herlach: Phase Transformations in Multicomponent Melts, Wiley-VCH Verlag GmbH & Co. KGaA, Weinheim, Germany, 2008.

[8] J. Brillo, I. Egry, J. Westphal: Int. J. Mat. Res. 99 (2008) 162.
[9] W.N. Eremenko, W.I. Nichenko, J.W. Naidich: Izw. Akad. Nauk. OTN 3 (1961) 150.
[10] P. Laty, J.C. Joud, P. Desre: Surf. Sci. 69 (1977) 508. DOI:10.1016/0039-6028(77)90130-3
[11] D.R. Poirier, R. Speiser: Met. Trans. A 18 (1987) 1156. DOI:10.1007/BF02647028
[12] D.M. Herlach, R.F. Cochrane, I. Egry, H.J. Fecht, A.L. Greer: Int. Mater. Rev. 38 (1993) 273.
[13] J. Brillo, G. Lohöfer, F. Schmidt-Hohagen, S. Schneider, I. Egry: J. Mat. Prod. Tech. 16 (2006) 247.
[14] I. Egry, J. Brillo, D. Holland-Moritz, Y. Plevachuk: Mater. Sci. Eng. 495 (2008) 14. DOI:10.1016/j.msea.2007.07.104
[15] Y. Plevachuk, I. Egry, J. Brillo, D. Holland-Moritz, I. Kaban: Int. J. Mat. Res. 98 (2007) 1526.
[16] J. Brillo, D. Chatain, I. Egry: Int. Mat. Res. 100 (2009) 53.
[17] J. Brillo, S.M. Chathoth, M.M. Koza, A. Meyer: Appl. Phys. Lett. 93 (2008) 121905. DOI:10.1063/1.2977863
[18] J.A.V. Butler: Proc. Roy. Soc. A 135 (1932) 348. DOI:10.1098/rspa.1932.0040
[19] T.P. Hoar, D.A. Melford: Trans. Farad. Soc. 33 (1957) 315. DOI:10.1039/tf9575300315
[20] T. Tanaka, T. Iida: Steel research 65 (1994) 21.
[21] T. Tanaka, K. Hack, T. Iida, S. Hara: Z. Metallkd. 87 (1996) 380.
[22] C. Antion, D. Chatain: Surf. Sci. 601 (2007) 2232. DOI:10.1016/j.susc.2007.03.026
[23] C. Lüdecke, D. Lüdecke: Thermodynamik, Springer, Heidelberg, BRD (2000) 506.
[24] V.T. Witusiewicz, U. Hecht, S.G. Fries, S. Rex: Journal of Alloys and Compounds 385 (2004) 133–143.
[25] N. Saunders: Al–Cu System, in: I. Ansara, A.T. Dinsdale, M.H. Rund (Eds.) COST-507; Thermochemical Database for Light Metal Alloys, European Communities, Luxembourg (1998) 28.
[26] M. Shimoji: Liquid Metals – An Introduction to the Physics and Chemistry of Metals in the Liquid State, Academic Press, London, 353, 1977.
[27] D.M. Herlach, I. Egry, P. Baeri, F. Spaepen (Eds.): Undercooled Metallic Melts: Properties, Solidification and Metastable Phases, Reprinted from Mat. Sci. Eng. A 178, Elsevier, The Netherlands, 1994.
[28] S. Krishnan, G.P. Hansen, R.H. Hauge, J.L. Margrave: High Temp. Sci. 29 (1990) 17.
[29] Lord Rayleigh: Proc. P. Soc. Lond. 29 (1879) 71.
[30] I. Egry, G. Lohöfer, S. Schneider, B. Feuerbacher: Appl. Phys. Lett. 73 (1998) 462. DOI:10.1063/1.121900
[31] D.L. Cummings, D.A. Blackburn: J. Fluid Mech. 224 (1991) 395. DOI:10.1017/S0022112091001817
[32] L. Goumiri, J.C. Joud: Acta Metall. 30 (1982) 1397. DOI:10.1016/0001-6160(82)90160-2
[33] P.A. Pamies, C. Garcia Cordovilla, E. Louis: Scripta Metall. 18 (1984) 869. DOI:10.1016/0036-9748(84)90251-5
[34] N. Eustathopoulos, M.G. Nicholas, B. Drevet: Wettability at High Temperatures, Pergamon Materials Series, New York, NY (1999).
[35] N.A. Watolin, O.A. Esin, W.F. Uchow, E.L. Dubinin: Trudy Inst. Met. Swardlowsk 18 (1969) 73.
[36] I.P. Yatsenko, W.I. Konomenko, A.L. Schukman: Tepl. Vysok Temp. (10) (1972) 66.
[37] G. Lang: Aluminium 50 (1974) 731.
[38] R.F. Brooks, K.C. Mills, I. Egry, D. Grant, S. Seetharaman, B. Vinet: Reference data for high temperature viscosity and surface tension data: NPL Report CMMT(D) 136 (1998).
[39] J. Brillo, I. Egry: J. Mat. Sci. 40 (2005) 2213. DOI:10.1007/s10853-005-1935-6
[40] P. Shen, H. Fujii, T. Matsumoto, K. Nogi: J. Mat. Sci. 40 (2005) 2329. DOI:10.1007/s10853-005-1954-3
[41] J.M. Molina, R. Voytovych, E. Louis, N. Eustathopoulos: Int. J. Adhesion & Adhesives 27 (2007) 394. DOI:10.1016/j.ijadhadh.2006.09.006
[42] M. Polak, L. Rubinovich: Surf. Sci. Reports 38 (200) 127.
[43] K. Mukai, T. Matsushita, K.C. Mills, S. Seetharaman, T. Furuzono: Met. Mater. Trans. B 39 (2008) 561. DOI:10.1007/s11663-008-9164-4

(Received March 10, 2009; accepted September 3, 2009)

**Bibliography**

DOI 10.3139/146.110221
Int. J. Mat. Res. (formerly Z. Metallkd.)
100 (2009) 11; page 1529–1535

ISSN 1862-5282

**Correspondence address**

Dr. Jürgen Brillo
Institut für Materialphysik im Weltraum
Deutsches Zentrum für Luft- und Raumfahrt (DLR)
51170 Köln, Germany
Tel.: +49 2203 601 2917
Fax: +49 2203 601 2255
E-Mail: Juergen.Brillo@dlr.de

You will find the article and additional material by entering the document number **MK110221** on our website at *www.ijmr.de*